Letter

Chiral Majorana hinge modes in superconducting Dirac materials

Bo Fu,[1] Zi-Ang Hu,[1] Chang-An Li,[2] Jian Li,[3,4] and Shun-Qing Shen[1,*]

[1]*Department of Physics, The University of Hong Kong, Pokfulam Road, Hong Kong, China*
[2]*Institute for Theoretical Physics and Astrophysics, University of Wurzburg, D-97074 Wurzburg, Germany*
[3]*School of Science, Westlake University, 18 Shilongshan Road, Hangzhou 310024, Zhejiang Province, China*
[4]*Institute of Natural Sciences, Westlake Institute for Advanced Study, 18 Shilongshan Road, Hangzhou 310024, Zhejiang Province, China*

(Received 3 November 2020; revised 15 March 2021; accepted 30 April 2021; published 13 May 2021)

Chiral Majorana hinge modes are characteristic of a second-order topological superconductor in three dimensions. Here we systematically study pairing symmetry and the leading pairing channels in Dirac materials with the point group D_{2h}, and find that the $s+id$-wave pairing superconductivity may exist as a consequence of competition between s- and d-wave pairing. The superconducting state is topologically nontrivial and possesses Majorana hinge and surface modes. The chiral Majorana hinge modes can be characterized by a winding number of the quadrupole moment or quantized quadruple moment at the symmetrically invariant point. Possible relevance to superconductivity in $ZrTe_5$ is discussed. Our findings suggest the strong spin-orbital coupling, crystalline symmetries, and electron-electron interaction in the Dirac materials may provide a platform to realize chiral Majorana hinge modes with no proximity effect or external fields.

DOI: 10.1103/PhysRevB.103.L180504

I. INTRODUCTION

Majorana modes are the quasiparticles around a topological superconductor and may have potential applications in topological quantum computations [1–6]. Over the last two decades, intensive efforts have been made to realize topological superconductors [7–13]. The Majorana edge modes in a p_x+ip_y spinless superconductor, a superconducting analog of quantum Hall effect state, move in a dissipationless and unidirectional way, i.e., are chiral because of the violation of time-reversal symmetry [14–17]. As the p-wave superconductor is rare in nature, a hybrid system of quantum anomalous Hall insulator and superconductor was alternatively proposed to realize the chiral topological superconductor [18–20]. However, the existence of chiral Majorana modes is still inconclusive [21–25], although several schemes for detection and application were proposed [26–28]. Those proposals often relied heavily on the proximity effect or needed an external magnetic field to break the time-reversal symmetry, which all made them difficult to be realized in experiments. Very recently, a significant advance in the research of topological quantum phases is a generalization to higher-order topological insulators and superconductors that can host localized modes near the corner, hinge, or vertex of a system [29–46]. Several theoretical proposals have been put forward to realize the Majorana corner modes in second-order topological superconductors [47–66]. In three dimensions, chiral Dirac modes can emerge along a hinge between two surface planes on which the two gapped surface modes encounter when the time-reversal symmetry is broken [67–70]. This opens a new avenue to research chiral Majorana modes in topological superconducting materials.

Here we investigate all possible superconducting pairing channels in three-dimensional (3D) massive Dirac materials with the D_{2h} point-group symmetry at the mean-field level with long-ranged interactions. We find that the leading pairing channel can be s-, d-, or $s+id$-wave pairing by varying the relative strength of the intra and interorbital interactions. The s-wave pairing is topologically nontrivial under time-reversal invariance and possesses a gapless Majorana surface mode as proposed by Fu and Berg [71] and Sato [72]. For the $s+id$-wave pairing channel, the inclusion of d_{xy}- wave pairing breaks either the time-reversal symmetry or inversion symmetry, but preserves the combination of these two symmetries. Consequently, the system becomes a second-order topological superconductor with chiral Majorana hinge modes circulating along the four hinges parallel to the z-axis. The topology behind chiral Majorana hinge modes can be characterized by a winding number of the quadrupole moment, or the quantized quadrupole moment at the particle-hole invariant momentum. This establishes a robust and new bulk-boundary correspondence for the topological states of matter. We also discuss its possible relevance to the superconductivity in a prototype of massive Dirac material $ZrTe_5$.

II. MODEL

We start with a normal state Hamiltonian for a 3D Dirac material with D_{2h} point-group symmetry and time-reversal symmetry

$$H_0=\sum_{\boldsymbol{k}}\Psi_{\boldsymbol{k}}^{\dagger}(h_{\boldsymbol{k}}-\mu)\tau_z\Psi_{\boldsymbol{k}} \tag{1}$$

*sshen@hku.hk

TABLE I. Eight classes of the basis of the pairing functions according to D_{2h} point-group symmetry. From left to right, each column shows the irreducible representations (IRs) of the point group D_{2h}, intraorbital or interorbital pairing, the pairing channels $\varphi_\Gamma(\boldsymbol{k})M_{ij}$ with antisymmetric matrices, the pairing functions $N_{\boldsymbol{k},\Gamma} = \varphi_{\Gamma'}(\boldsymbol{k})U_{\boldsymbol{k}}^\dagger M_{ij}U_{\boldsymbol{k}}$ with $U_{\boldsymbol{k}}$ being a 4×2 matrix of conduction band eigenvectors [78], and the average over the Fermi surface $\langle N_{\boldsymbol{k},\Gamma}^2\rangle$. The Pauli matrices $\widetilde{\sigma}_i$ denote the Kramers-degenerated conduction bands and we introduced the notation $\boldsymbol{p} = (v_x k_x, v_y k_y, v_z k_z)$. The Fermi-surface harmonics $\varphi_0 = 1$ and $\varphi_{ij} = \frac{\sqrt{15}}{1-m^2/\mu^2}\frac{v_i v_j k_i k_j}{\epsilon_{\boldsymbol{k}}^2}$ with $\epsilon_{\boldsymbol{k}} = \sqrt{\sum_i v_i^2 k_i^2 + m^2}$.

IRs	orbital	$\varphi_\Gamma(\boldsymbol{k})M_{ij}$	$N_{\boldsymbol{k},\Gamma}$	$\langle N_{\boldsymbol{k},\Gamma}^2\rangle$
A_g	intra	$\varphi_0\sigma_0 s_0$	$\varphi_0\widetilde{\sigma}_0$	1
B_{1g}	intra	$\varphi_{xy}\sigma_0 s_0$	$\varphi_{xy}\widetilde{\sigma}_0$	1
B_{2g}	intra	$\varphi_{xz}\sigma_0 s_0$	$\varphi_{xz}\widetilde{\sigma}_0$	1
B_{3g}	intra	$\varphi_{yz}\sigma_0 s_0$	$\varphi_{yz}\widetilde{\sigma}_0$	1
A_u	inter	$\varphi_0\sigma_x s_0$	$\varphi_0\frac{\boldsymbol{p}\cdot\widetilde{\boldsymbol{\sigma}}}{\epsilon_{\boldsymbol{k}}}$	$1-\frac{m^2}{\mu^2}$
B_{1u}	inter	$\varphi_0\sigma_y s_z$	$\varphi_0\frac{(\boldsymbol{p}\times\widetilde{\boldsymbol{\sigma}})_z}{\epsilon_{\boldsymbol{k}}}$	$\frac{2}{3}(1-\frac{m^2}{\mu^2})$
B_{2u}	inter	$\varphi_0\sigma_y s_y$	$\varphi_0\frac{(\boldsymbol{p}\times\widetilde{\boldsymbol{\sigma}})_y}{\epsilon_{\boldsymbol{k}}}$	$\frac{2}{3}(1-\frac{m^2}{\mu^2})$
B_{3u}	inter	$\varphi_0\sigma_y s_x$	$\varphi_0\frac{(\boldsymbol{p}\times\widetilde{\boldsymbol{\sigma}})_x}{\epsilon_{\boldsymbol{k}}}$	$\frac{2}{3}(1-\frac{m^2}{\mu^2})$

in the Nambu spinor basis $\Psi_{\boldsymbol{k}} = (\psi_{\boldsymbol{k}}, -is_y\psi_{-\boldsymbol{k}}^*)$, where $\psi_{\boldsymbol{k}}$ is a four-component Dirac spinor. In the $\mathbf{k}\cdot\mathbf{p}$ theory, $h_{\boldsymbol{k}} = \sum_{i=x,y,z} v_i k_i\sigma_x s_i + m\sigma_z s_0$ with $v_{x,y,z}$ being the velocities along three directions, m the Dirac mass, and $\boldsymbol{s}$, $\boldsymbol{\sigma}$ and $\boldsymbol{\tau}$ the Pauli matrices acting on spin, orbital, and Nambu space, respectively [73,74], ($\hbar = 1$). Here μ is the chemical potential. Furthermore, we consider the phonon-mediated effective electron-electron interaction. Due to the multiorbital nature of the Dirac electron, there are two distinct electron-phonon coupling mechanisms. The first is the deformation-potential coupling induced by the local dilation of the lattice, which appears as the diagonal components in the orbital space. The second one is an effective gauge field or vector potential coupling induced by the shear deformation, which appears as the hopping matrix elements in the orbital space. Generally speaking, the exchange and pairing-hopping terms are rather small compared with the intra and interorbital terms, thus can be neglected. By utilizing the Fierz identity [75–78], the density-density product of four-fermion interaction can be decomposed into the pairing terms

$$H_{\text{int}} = \sum_{\boldsymbol{k},\boldsymbol{k}',i,j}\frac{V_i(\boldsymbol{k}-\boldsymbol{k}')}{8\Omega}[\Psi_{\boldsymbol{k}}^\dagger\tau_+ M_{ij}\Psi_{\boldsymbol{k}}][\Psi_{\boldsymbol{k}'}^\dagger\tau_- M_{ij}\Psi_{\boldsymbol{k}'}], \quad (2)$$

where Ω is the volume of the sample, $M_{ij}\equiv\sigma_i s_j$, and $\tau_\pm = \frac{1}{2}(\tau_x \pm i\tau_y)$. The interaction potential $V_i(\boldsymbol{k}-\boldsymbol{k}')$ can be decomposed by the Fermi-surface harmonics $\varphi_\Gamma(\boldsymbol{k})$ for each irreducible representation of the crystal point group $V_i(\boldsymbol{k}-\boldsymbol{k}') = \sum_\Gamma V_i^\Gamma\varphi_\Gamma(\boldsymbol{k})[\varphi_\Gamma(\boldsymbol{k}')]^*$ [78,79] where the sum over Γ contains all nonequivalent irreducible representations (IRs) of the D_{2h} group [80]. The basis functions for each IR are clearly not unique, and have been truncated to the lowest order in momenta for simplicity [78]. The overall pairing functions are constructed by the orbital angular momentum part $\varphi_\Gamma(\boldsymbol{k})$ and spin-orbital part M_{ij} listed in Table I. Here we only focus on the regime with the even s- and d-wave pairing function $[\varphi_\Gamma(\boldsymbol{k}) = \varphi_\Gamma(-\boldsymbol{k})$] for the orbital part, which restricts ourselves to the remaining six antisymmetric pairing matrices M_{ij}, i.e., $[M_{ij}(-is_y)]^T = -M_{ij}(-is_y)$ due to the Fermi-Dirac statistics. As a result of products of representations, the overall paring function $\varphi_\Gamma(\boldsymbol{k})M_{ij}$ and the orbital angular momentum part $\varphi_\Gamma(\boldsymbol{k})$ may belong to different IRs.

III. DETERMINATION OF THE PAIRING SYMMETRY

Now we evaluate the transition temperature T_c^Γ for each pairing channel listed in Table I. It can be obtained by solving the linearized gap equation near the transition temperature T_c at which the order parameter is vanishingly small. Generally speaking, $T_c^\Gamma \simeq 1.13\omega_D\exp[-\frac{1}{\lambda_\Gamma\langle N_{\boldsymbol{k},\Gamma}^2\rangle}]$ associated with each IR can be different. The transition temperature is dictated by two factors. The first one is the average of the square of the projected pairing matrix $\langle N_{\boldsymbol{k},\Gamma}^2\rangle$ over the Fermi surface. The second one is the dimensionless coupling strength $\lambda_\Gamma = 2g_\Gamma\rho(\mu)$ with the effective interaction g_Γ and the density of states $\rho(\mu)$ near the Fermi level. The interorbital interaction $V_{i=x,y}(\boldsymbol{r}-\boldsymbol{r}')$ and the intraorbital interaction $V_{i=0,z}(\boldsymbol{r}-\boldsymbol{r}')$ give rise to pairing in the odd-parity channels $(A_u, B_{1u}, B_{2u}, B_{3u})$ and even-parity channels $(A_g, B_{1g}, B_{2g}, B_{3g})$, respectively. The four odd-parity pairing channels are generated from the local interorbital interaction and the transition temperatures satisfy $T_c^{A_u} \gg T_c^{B_{1u}}, T_c^{B_{2u}}, T_c^{B_{3u}}$. Thus we need only to consider the s-wave superconductivity belonging to the A_u representation among the four odd-parity pairing channels. Without loss of generality, we assume $g_{B_{1g}} > g_{B_{2g}} > g_{B_{3g}}$. Under this condition, it is unlikely for the system to form the order parameter in B_{2g} and B_{3g} channels. Depending on the pairing interaction, we cannot avoid the possibility of the pairing belonging to the A_g representation. Since this order parameter breaks no additional symmetries besides the $U(1)$ gauge symmetry, we disregard this conventional pairing for the further discussions. We also checked numerically that the conclusion remains unchanged even with the inclusion of this pairing.

From now on, we focus on the topological nontrivial phases with s- and d-wave pairing which belong to two different irreducible representations A_u and B_{1g}, respectively. Generally, the superconductivity order parameter for each IR η_Γ is complex which can be parameterized as $\eta_\Gamma = |\eta_\Gamma|e^{i\phi_\Gamma}$. By minimizing the free energy with the two superconducting order parameters, the relative phase should to be $\Delta\phi = \pm\pi/2$ if they coexist [78]. Then the pairing function can be expressed as $\sum_\Gamma \eta_\Gamma N_{\boldsymbol{k}}^\Gamma = \eta_{A_u}N_{\boldsymbol{k},A_u} - i\eta_{B_{1g}}N_{\boldsymbol{k},B_{1g}}$, with $N_{\boldsymbol{k},A_u} = \varphi_0\frac{\boldsymbol{p}\cdot\widetilde{\boldsymbol{\sigma}}}{\epsilon_{\boldsymbol{k}}}$ and $N_{\boldsymbol{k},B_{1g}} = \varphi_{xy}\widetilde{\sigma}_0$. Thus, the projected Bogoliubov–de Gennes Hamiltonian is

$$\widetilde{h}_{\boldsymbol{k}}^{\text{BdG}} = (\epsilon_{\boldsymbol{k}}-\mu)\widetilde{\sigma}_0\tau_z + \frac{\eta_{A_u}}{\mu}\boldsymbol{p}\cdot\widetilde{\boldsymbol{\sigma}}\tau_x + \frac{\sqrt{15}\eta_{B_{1g}}v_x v_y k_x k_y}{\mu^2-m^2}\widetilde{\sigma}_0\tau_y. \quad (3)$$

The gap equations are reduced to a pair of coupled self-consistent equations of superconducting gap for the two paring amplitudes $\eta_{A_u}(T)$ and $\eta_{B_{1g}}(T)$.

IV. $s + id$ WAVE PAIRING STATE

Now we turn to explore the possibility of a mixed $s + id$-wave pairing superconductivity which breaks the

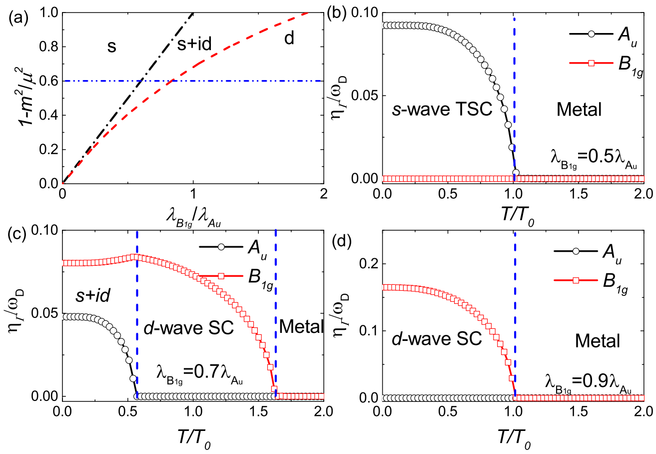

FIG. 1. (a) Zero-temperature phase diagram as a function of $1-m^2/\mu^2$ and $\lambda_{B_{1g}}/\lambda_{A_u}$. The temperature dependence order parameter (b) η_{A_u} for s-wave pairing (black lines with open circles), (d) $\eta_{B_{1g}}$ for d-wave pairing (red lines with open squares), and (c) for $s+id$-wave pairing. λ_{A_u} is set to be 1/2 and $1-m^2/\mu^2=0.6$. For regimes (b) and (d) with single-order parameter, the temperature is in the unit of its transition temperature $T_0=T_c^\Gamma$. For the mixed pairing regime (c), $T_0=T_c^{A_u}$.

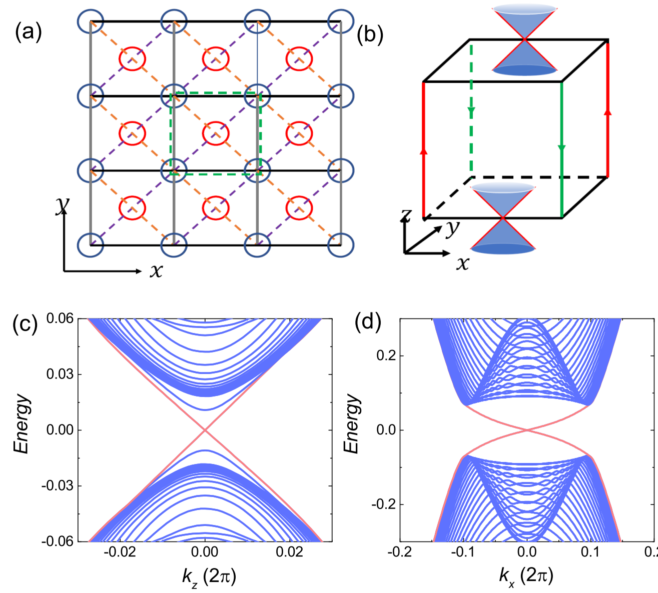

FIG. 2. (a) Schematic of cross-section lattice and the boundary of the x-y plane. The unit cell (the dash green box) consists of two sublattices indicated by blue and red circles. (b) The schematic of Majorana hinge modes and gapless Majorana surface modes in the case of $s+id$-wave pairing. (c) The dispersion spectrum of Majorana hinge modes for quasi-1D hinges along z direction with $L_x=L_y=60$. (d) The dispersion spectrum of the Majorana surface modes in the x-y plane. The open boundary condition is adopted along z direction with the height $L_z=200$ and the periodic boundaries are adopted along x and y directions(see Sec. VII of Ref. [78]). The chemical potential $\mu=0.5$.

time-reversal symmetry spontaneously. The type of mixed pairing has been discussed in cuprates [81,82] and iron pnictides [83–85]. Figure 1(a) shows the phase diagram at zero temperature as a function of $1-m^2/\mu^2$ and the interaction ratio $\lambda_{B_{1g}}/\lambda_{A_u}$ with fixed λ_{A_u} to illustrate the competition between the s- and d-wave pairing superconductivity. The red and black dotted lines indicate the phase boundary separating the purely s- or d-wave pairing and the mixed $s+id$-wave pairing. The competition between the s- and d-wave pairing channels can lead to either a purely s- or d-wave pairing state, or a mixed $s+id$-wave state. The mixed $s+id$-wave pairing state may appear at the intermediate region $-\frac{14}{15}\lambda_{A_u} < \lambda_{A_u}/\lambda_{B_{1g}}-(1-m^2/\mu^2)^{-1}<0$. It is intuitively clear that for such an $s+id$-solution to be held, the pairing strengths λ_{A_u} and $\lambda_{B_{1g}}$ need to be comparable: otherwise, a s-wave or a d-wave will dominate. Adjusting the chemical potential toward the band edge, the region for the mixed pairing shrinks. Thus, the mixed pairing is more likely to occur in a system when the chemical potential is located away from the band edge.

Then we discuss the behaviors of two different order parameters η_{A_u} and $\eta_{B_{1g}}$ at finite temperatures, which are calculated by solving the gap equations as a function of temperature for several values of $\lambda_{B_{1g}}/\lambda_{A_u}$ and fixed $m^2/\mu^2=0.4$. Figures 1(b) to 1(d) show the temperature dependence of the order parameters in the s-, mixed $s+id$-, and d-wave pairing states, respectively. For the pure s- and d-wave pairing states, the superconducting transition is only specific to one of the IRs and the critical temperature is precisely determined by T_c^Γ. For the mixed pairing state ($\lambda_{B_{1g}}/\lambda_{A_u}=0.7$), as the temperature decreases down to a certain value $\sim 1.63T_0$, the d-wave pairing $\eta_{B_{1g}}$ first appears. After that, the s-wave pairing η_{A_u} appears and $\eta_{B_{1g}}$ increases gradually with temperature until $\sim 0.55T_0$. The d-wave component reduces while the s-wave component grows up as the temperature decreases to zero. This indicates that, with decreasing the temperature, it undergoes a topological phase transition from pure d-wave to $s+id$-wave superconductivity in specific conditions. Thus the $s+id$-wave superconductivity can exist at low temperatures.

V. MAJORANA HINGE AND SURFACE MODES IN THE $s+id$ WAVE PAIRING STATE

The $s+id$-wave pairing superconducting state is higher-order topologically nontrivial, which is revealed from the existence of Majorana hinge and surface modes. We adopt the tight-binding approximation on a cubic lattice with the lattice orientation of the x-y plane as shown in Fig. 2(a) [78]. Four chiral Majorana hinge modes and two Majorana surface modes are illustrated in Fig. 2(b). The origin of the topological hinge modes in the state can be heuristically explained in the following picture. According to the odd-parity superconductivity criterion [71], the system of the single s-wave paring (A_u) should be a time-reversal-invariant topological superconductor with massless helical Majorana modes on the surface. The inclusion of the d-wave order parameter gaps out the Dirac cones of the Majorana surface modes on the surfaces parallel to the z-axis as its relative $\pi/2$ phase to the s-wave order parameter breaks the time reversal symmetry. However, the d-wave pairing gap function vanishes at the mirror planes and acts as mass domain walls for Majorana surface modes. Consequently, the chiral Majorana hinge modes are formed around the domain wall or along the hinges. The dispersion

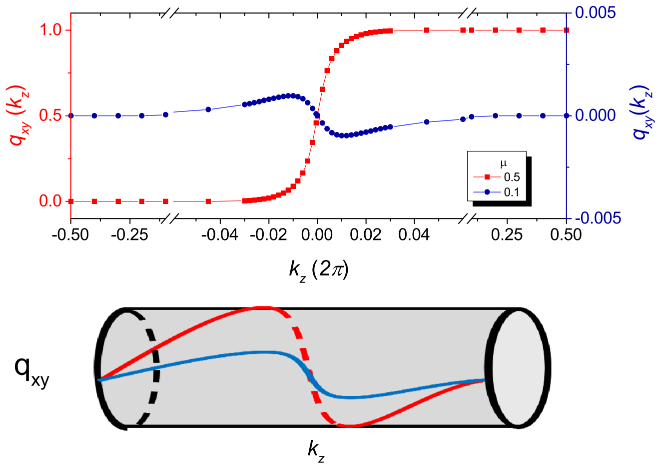

FIG. 3. The quadrupole moment $q_{xy}(k_z)$ as a function of k_z for $\mu = 0.5$ (red) with the winding number $\Delta q_{xy} = 1$ and $\mu = 0.1$ (blue) with $\Delta q_{xy} = 0$. The bottom: q_{xy} is rolled as a tube with q_{xy} module 1. The other parameters used are the same as Fig. 2.

spectra for the Majorana hinge states as a function of k_z are presented in Fig. 2(c). The gapless Majorana hinge modes in the gap are marked by the red lines and localized near the four hinges along the z-direction. Their dispersions are linear in k_z, $E_{\text{hinge}} = \pm\frac{\eta_{A_u}}{\mu}v_z k_z$, obtained from the projected Hamiltonian in Eq. (3). On the top and bottom surfaces of the x-y plane, the d-wave pairing breaks the time-reversal symmetry, but does not open the band gap of surface Majorana states. The dispersion spectra are plotted in Fig. 2(d), in which the gapless Majorana surface states are marked by the red lines. The BdG Hamiltonian with the odd-parity s-wave pairing ($\propto \sigma_x\tau_x$) possesses the time-reversal symmetry $\mathcal{T} = is_y\mathcal{K}$ and the inversion symmetry $\widetilde{\mathcal{I}} \equiv \mathcal{I}\tau_z = \sigma_z\tau_z$. The inclusion of the d-wave pairing ($\propto k_xk_y\tau_y$) breaks either $\mathcal{T}$ or $\widetilde{\mathcal{I}}$, but preserves $\widetilde{\mathcal{I}}\mathcal{T}$. This combined symmetry makes the Majorana hinge modes at diagonal hinges and the Majorana surface states at the opposite surface related by the symmetry operation $\widetilde{\mathcal{I}}\mathcal{T}$.

VI. TOPOLOGICAL INVARIANTS

Now we come to establish the bulk-hinge correspondence to connect the Majorana hinge modes to the topology of the bulk band structure. We take the periodic condition along the z axis such that k_z is still a good quantum number. The quadrupole moment for each k_z-sliced layer is given by [86–88]

$$q_{xy}(k_z) = \frac{1}{2\pi}\text{Im}\log\left[\text{Det}[U_{k_z}^{\dagger}QU_{k_z}]\sqrt{\text{Det}Q^{\dagger}}\right], \quad (4)$$

where the matrix U_{k_z} is constructed by the occupied ground states, $Q = e^{2\pi i\hat{x}\hat{y}/L_xL_y}$, $\hat{x}$ and $\hat{y}$ are the position operators, and L_x and L_y the length of our system in the x and y directions, respectively. Generally the particle-hole symmetry $\mathcal{P}$ is broken for a specific k_z as the two states at k_z and $-k_z$ are connected by the symmetry. However, the symmetry restores at $k_z = 0$ and π (half of the reciprocal lattice vector), i.e., the particle-hole invariant momentum. At these momenta, we can prove that the quadrupole moment q_{xy} is quantized to be 0 or 1/2 module 1 [78]. The quantized quadrupole moment of $q_{xy} = 1/2$ means the existence of the corner states of zero energy, a signature of the second-order topological phase in two dimensions [29,30]. The quantization is removed once k_z moves away from the invariant momentum. Additions of the corner states for different k_z evolve into the chiral hinge states in three dimensions with a linear dispersion crossing the point of $k_z = 0$. Furthermore, the symmetry $\mathcal{P}$ connects the unoccupied states at momentum k_z with unoccupied states at $-k_z$, which gives $q_{xy}(k_z) + q_{xy}(-k_z) = 0$ for a trivial case and 1 for a nontrivial case. Thus in the $s + id$-wave pairing state, a winding number can be introduced $\Delta q_{xy} = \int_{-\pi}^{\pi} dk_z\partial_{k_z}q_{xy}(k_z)$. Two k_z-dependent quadrupole moments for the trivial (blue line with circle) and nontrivial (red line with square) cases are plotted in Fig. 3. For $\mu = 0.5$, $q_{xy} = 1/2$ at $k_z = 0$, and 0 at $k_z = \pi$. Thus, the winding number $\Delta q_{xy} = 1$, which indicates the state is topologically nontrivial and is related to the presence of chiral Majorana hinge modes. In this way, we establish a bulk-hinge correspondence in the topologically nontrivial superconducting state.

VII. POSSIBLE RELEVANCE TO $ZrTe_5$

The transition-metal pentatelluride $ZrTe_5$ is the prototype of massive Dirac materials with finite band gaps whose low-energy excitations near the Fermi level are well described by the Hamiltonian (1) [89–92]. External pressure may reduce some of the crystalline symmetries of the system while preserving both the inversion symmetry and time reversal symmetry, thus the Kramers degeneracy of the bands remains. Under the high pressure, $ZrTe_5$ crystal can undergo a structural phase transition accompanied with its space group changing from the orthorhombic $Cmcm$ (D_{2h}) to monoclinic $C2/m$ (C_{2h}), then to triclinic $P-1$ (C_i) phases. The IRs of higher-symmetry point group will collapse into the IRs of point group with lower symmetry [78]. The two superconducting order parameters have opposite parities and fall into two different IRs. Furthermore, using a perturbative analysis [78], we find the critical temperatures for these two pairing channels can be enhanced by the external pressure when the band gap tends to be closed by increasing the pressure. It is anticipated that the external pressure may promote the formation of mixed $s + id$-wave pairing superconductivity in $ZrTe_5$, which is the regime we focused on in our work. The pressure-induced superconductivity was already reported experimentally in $ZrTe_5$ [93]. A two-step-like transition in the resistance measurement is observed, indicating the possible coexistence of the two superconducting phases. More substantial evidence will be anticipated to draw a conclusion.

ACKNOWLEDGMENTS

This work was supported by the Research Grants Council, University Grants Committee, Hong Kong under Grant No. 17301220; the National Key R&D Program of China under Grant No. 2019YFA0308603; Natural Science Foundation of China under Grant No. 11774317; and Natural Science Foundation of Zhejiang under Grant No. LQ20A040003.

[1] A. Yu Kitaev, Fault-tolerant quantum computation by anyons, Ann. Phys. (Amsterdam) **303**, 2 (2003).

[2] C. Nayak, S. H. Simon, A. Stern, M. Freedman, and S. Das Sarma, Non-Abelian anyons and topological quantum computation, Rev. Mod. Phys. **80**, 1083 (2008).

[3] F. Wilczek, Majorana returns, Nat. Phys. **5**, 614 (2009).

[4] J. Alicea, New directions in the pursuit of Majorana fermions in solid state systems, Rep. Prog. Phys. **75**, 076501 (2012).

[5] C. W. J. Beenakker, Search for Majorana fermions in superconductors, Annu. Rev. Condens. Matter Phys. **4**, 113 (2013).

[6] S. R. Elliott and M. Franz, Colloquium: Majorana fermions in nuclear, particle, and solid-state physics, Rev. Mod. Phys. **87**, 137 (2015).

[7] V. Mourik, K. Zuo, S. M. Frolov, S. R. Plissard, E. P. A. M. Bakkers, and L. P. Kouwenhoven, Signatures of Majorana fermions in hybrid superconductor-semiconductor nanowire devices, Science **336**, 1003 (2012).

[8] A. Das, Y. Ronen, Y. Most, Y. Oreg, M. Heiblum, and H. Shtrikman, Zero-bias peaks and splitting in an Al-InAs nanowire topological superconductor as a signature of Majorana fermions, Nat. Phys. **8**, 887 (2012).

[9] L. P. Rokhinson, X. Liu, and J. K. Furdyna, The fractional a.c. Josephson effect in a semiconductor-superconductor nanowire as a signature of Majorana particles, Nat. Phys. **8**, 795 (2012).

[10] S. Nadj-Perge, I. K. Drozdov, J. Li, H. Chen, S. Jeon, J. Seo, A. H. MacDonald, B. A. Bernevig, and A. Yazdani, Observation of Majorana fermions in ferromagnetic atomic chains on a superconductor, Science **346**, 602 (2014).

[11] H.-H. Sun, K.-W. Zhang, L.-H. Hu, C. Li, G.-Y. Wang, H.-Y. Ma, Z.-A. Xu, C.-L. Gao, D.-D. Guan, Y.-Y. Li, C. Liu, D. Qian, Y. Zhou, L. Fu, S.-C. Li, F.-C. Zhang, and J.-F. Jia, Majorana Zero Mode Detected with Spin Selective Andreev Reflection in the Vortex of a Topological Superconductor, Phys. Rev. Lett. **116**, 257003 (2016).

[12] D. Wang, L. Kong, P. Fan, H. Chen, S. Zhu, W. Liu, L. Cao, Y. Sun, S. Du, J. Schneeloch, R. Zhong, G. Gu, L. Fu, H. Ding, and H.-J. Gao, Evidence for Majorana bound states in an iron-based superconductor, Science **362**, 333 (2018).

[13] R. M. Lutchyn, E. P. A. M. Bakkers, L. P. Kouwenhoven, P. Krogstrup, C. M. Marcus, and Y. Oreg, Majorana zero modes in superconductor-semiconductor heterostructures, Nat. Rev. Mater. **3**, 52 (2018).

[14] G. E. Volovik, Fermion zero modes on vortices in chiral superconductors, J. Exp. Theor. Phys. Lett. **70**, 609 (1999).

[15] N. Read and D. Green, Paired states of fermions in two dimensions with breaking of parity and time-reversal symmetries and the fractional quantum Hall effect, Phys. Rev. B **61**, 10267 (2000).

[16] D. A. Ivanov, Non-Abelian Statistics of Half-Quantum Vortices in p-wave Superconductors, Phys. Rev. Lett. **86**, 268 (2001).

[17] A. Yu Kitaev, Unpaired Majorana fermions in quantum wires, Phys. Usp. **44**, 131 (2001).

[18] X.-L. Qi, T. L. Hughes, and S.-C. Zhang, Chiral topological superconductor from the quantum Hall state, Phys. Rev. B **82**, 184516 (2010).

[19] S. B. Chung, X.-L. Qi, J. Maciejko, and S.-C. Zhang, Conductance and noise signatures of Majorana backscattering, Phys. Rev. B **83**, 100512(R) (2011).

[20] J. Wang, Q. Zhou, B. Lian, and S.-C. Zhang, Chiral topological superconductor and half-integer conductance plateau from quantum anomalous Hall plateau transition, Phys. Rev. B **92**, 064520 (2015).

[21] Q. L. He, L. Pan, A. L. Stern, E. Burks, X. Che, G. Yin, J. Wang, B. Lian, Q. Zhou, E. S. Choi, K. Murata, X. Kou, T. Nie, Q. Shao, Y. Fan, S.-C. Zhang, K. Liu, J. Xia, and K. L. Wang, Chiral Majorana fermion modes in a quantum anomalous Hall insulator–superconductor structure, Science **357**, 294 (2017).

[22] W. Ji and X.-G. Wen, $1/2(e^2/h)$ Conductance Plateau without 1D Chiral Majorana Fermions, Phys. Rev. Lett. **120**, 107002 (2018).

[23] Y. Huang, F. Setiawan, and J. D. Sau, Disorder-induced half-integer quantized conductance plateau in quantum anomalous Hall insulator-superconductor structures, Phys. Rev. B **97**, 100501(R) (2018).

[24] B. Lian, J. Wang, X.-Q. Sun, A. Vaezi, and S.-C. Zhang, Quantum phase transition of chiral Majorana fermions in the presence of disorder, Phys. Rev. B **97**, 125408 (2018).

[25] M. Kayyalha, D. Xiao, R. Zhang, J. Shin, J. Jiang, F. Wang, Y.-F. Zhao, R. Xiao, L. Zhang, K. M. Fijalkowski, P. Mandal, M. Winnerlein, C. Gould, Q. Li, L. W. Molenkamp, M. H. W. Chan, N. Samarth, and C.- Z. Chang, Absence of evidence for chiral Majorana modes in quantum anomalous Hall-superconductor devices, Science **367**, 64 (2020).

[26] G. Struebi, W. Belzig, M.-S. Choi, and C. Bruder, Interferometric and Noise Signatures of Majorana Fermion Edge States in Transport Experiments, Phys. Rev. Lett. **107**, 136403 (2011).

[27] B. Lian, X.-Q. Sun, A. Vaezi, X.-L. Qi, and S.-C. Zhang, Topological quantum computation based on chiral Majorana fermions, Proc. Natl. Acad. Sci. USA **115**, 10938 (2018).

[28] C. A. Li, J. Li, and S.-Q. Shen, Majorana-Josephson interferometer, Phys. Rev. B **99**, 100504(R) (2019).

[29] W. A. Benalcazar, B. Andrei Bernevig, and T. L. Hughes, Quantized electric multipole insulators, Science **357**, 61 (2017).

[30] W. A. Benalcazar, B. Andrei Bernevig, and T. L. Hughes, Electric multipole moments, topological multipole moment pumping, and chiral hinge states in crystalline insulators, Phys. Rev. B **96**, 245115 (2017).

[31] F. Schindler, A. M. Cook, M. G. Vergniory, Z. Wang, S. S. P. Parkin, B. Andrei Bernevig, and T. Neupert, Higher-order topological insulators, Sci. Adv. **4**, eaat0346 (2018).

[32] X. Zhu, Second-Order Topological Superconductors with Mixed Pairing, Phys. Rev. Lett. **122**, 236401 (2019).

[33] J. Langbehn, Y. Peng, L. Trifunovic, F. von Oppen, and P. W. Brouwer, Reflection-Symmetric Second-order Topological Insulators and Superconductors, Phys. Rev. Lett. **119**, 246401 (2017).

[34] M. Ezawa, Higher-Order Topological Insulators and Semimetals on the Breathing Kagome and Pyrochlore Lattices, Phys. Rev. Lett. **120**, 026801 (2018).

[35] E. Khalaf, Higher-order topological insulators and superconductors protected by inversion symmetry, Phys. Rev. B **97**, 205136 (2018).

[36] S. Franca, J. van den Brink, and I. C. Fulga, An anomalous higher-order topological insulator, Phys. Rev. B **98**, 201114(R) (2018).

[37] D. Călugăru, V. Juričić, and B. Roy, Higher-order topological phases: A general principle of construction, Phys. Rev. B **99**, 041301(R) (2019).
[38] C. A. Li and S. S. Wu, Topological states in generalized electric quadrupole insulators, Phys. Rev. B **101**, 195309 (2020).
[39] F. Schindler, Z. Wang, M. G. Vergniory, A. M. Cook, A. Murani, S. Sengupta, A. Yu Kasumov, R. Deblock, S. Jeon, I. Drozdov, H. Bouchiat, S. Guéron, A. Yazdani, B. A. Bernevig, and T. Neupert, Higher-order topology in bismuth, Nat. Phys. **14**, 918 (2018).
[40] S. Imhof, C. Berger, F. Bayer, J. Brehm, L. W. Molenkamp, T. Kiessling, F. Schindler, C. Hua Lee, M. Greiter, T. Neupert, and R. Thomale, Topolectrical-circuit realization of topological corner modes, Nat. Phys. **14**, 925 (2018).
[41] M. Serra-Garcia, V. Peri, R. Süsstrunk, O. R. Bilal, T. Larsen, L. G. Villanueva, and S. D. Huber, Observation of a phononic quadrupole topological insulator, Nature (London) **555**, 342 (2018).
[42] C. W. Peterson, W. A. Benalcazar, T. L. Hughes, and G. Bahl, A quantized microwave quadrupole insulator with topologically protected corner states, Nature (London) **555**, 346 (2018).
[43] X. Zhang, H.-X. Wang, Z.-K. Lin, Y. Tian, B. Xie, M.-H. Lu, Y.-F. Chen, and J.-H. Jiang, Second-order topology and multidimensional topological transitions in sonic crystals, Nat. Phys. **15**, 582 (2019).
[44] M. Kheirkhah, Z. Yan, Y. Nagai, and F. Marsiglio, First- and Second-Order Topological Superconductivity and Temperature-Driven Topological Phase Transitions in the Extended Hubbard Model with Spin-Orbit Coupling, Phys. Rev. Lett. **125**, 017001 (2020).
[45] J. Niu, T. Yan, Y. Zhou, Z. Tao, X. Li, W. Liu, L. Zhang, S. Liu, Z. Yan, Y. Chen, and D. Yu, Simulation of higher-order topological phases and related topological phase transitions in a superconducting qubit, arXiv:2001.03933 [Sci. Bull. (to be published)].
[46] R.-X. Zhang, Y.-T. Hsu, and S. Das Sarma, Higher-order topological Dirac superconductors, Phys. Rev. B **102**, 094503 (2020).
[47] Z. Yan, F. Song, and Z. Wang, Majorana Kramers Pairs in a High-Temperature Tlatform, Phys. Rev. Lett. **121**, 096803 (2018).
[48] Y. Wang, M. Lin, and T. L. Hughes, Weak-pairing higher order topological superconductors, Phys. Rev. B **98**, 165144 (2018).
[49] Q. Wang, C.-C. Liu, Y.-M. Lu, and F. Zhang, High Temperature Majorana Corner States, Phys. Rev. Lett. **121**, 186801 (2018).
[50] Z. Wu, Z. Yan, and W. Huang, Higher-order topological superconductivity: Possible realization in Fermi gases and Sr_2RuO_4, Phys. Rev. B **99**, 020508(R) (2019).
[51] C.-H. Hsu, P. Stano, J. Klinovaja, and D. Loss, Majorana Kramers Pairs in Higher-Order Topological Insulators, Phys. Rev. Lett. **121**, 196801 (2018).
[52] T. Liu, J. J. He, and F. Nori, Majorana corner states in a two-dimensional magnetic topological insulator on a high-temperature superconductor, Phys. Rev. B **98**, 245413 (2018).
[53] Y. Volpez, D. Loss, and J. Klinovaja, Second-Order Topological Superconductivity in π-Junction Rashba Layers, Phys. Rev. Lett. **122**, 126402 (2019).
[54] R.-X. Zhang, W. S. Cole, and S. Das Sarma, Helical Hinge Majorana Modes in Iron-Based Superconductors, Phys. Rev. Lett. **122**, 187001 (2019).
[55] C. Zeng, T. D. Stanescu, C. Zhang, V. W. Scarola, and S. Tewari, Majorana Corner Modes with Solitons in an Attractive Hubbard-Hofstadter Model of Cold Atom Optical Lattices, Phys. Rev. Lett. **123**, 060402 (2019).
[56] Z. Yan, Higher-Order Topological Odd-Parity Superconductors, Phys. Rev. Lett. **123**, 177001 (2019).
[57] S.-B. Zhang and B. Trauzettel, Detection of second-order topological superconductors by Josephson junctions, Phys. Rev. Research **2**, 012018(R) (2020).
[58] X.-H. Pan, K.-J. Yang, L. Chen, G. Xu, C.-X. Liu, and X. Liu, Lattice-Symmetry-Assisted Second-Order Topological Superconductors and Majorana Patterns, Phys. Rev. Lett. **123**, 156801 (2019).
[59] S. Franca, D. V. Efremov, and I. C. Fulga, Phase-tunable second-order topological superconductor, Phys. Rev. B **100**, 075415 (2019).
[60] R.-X. Zhang, W. S. Cole, X. Wu, and S. Das Sarma, Higher-Order Topology and Nodal Topological Superconductivity in Fe(Se, Te) Heterostructures, Phys. Rev. Lett. **123**, 167001 (2019).
[61] J. Ahn and B.-J. Yang, Higher-order topological superconductivity of spin-polarized fermions, Phys. Rev. Research **2**, 012060(R) (2020).
[62] M. Kheirkhah, Y. Nagai, C. Chen, and F. Marsiglio, Majorana corner flat bands in two-dimensional secondorder topological superconductors, Phys. Rev. B **101**, 104502 (2020).
[63] S. Ali Akbar Ghorashi, T. L. Hughes, and E. Rossi, Vortex and Surface Phase Transitions in Superconducting Higherorder Topological Insulators, Phys. Rev. Lett. **125**, 037001 (2020).
[64] Y.-T. Hsu, W. S. Cole, R.-X. Zhang, and J. D. Sau, Inversion-Protected Higher Order Topological Superconductivity in Monolayer WTe2, Phys. Rev. Lett. **125**, 097001 (2020).
[65] B. Roy, Higher-order topological superconductors in $\mathscr{P}$-, $\mathscr{T}$ -odd quadrupolar Dirac materials, Phys. Rev. B **101**, 220506(R) (2020).
[66] S.-B. Zhang, A. Calzona, and B. Trauzettel, All-electrically tunable networks of Majorana bound states, Phys. Rev. B **102**, 100503(R) (2020).
[67] B. Jäck, Y. L. Xie, J. Li, S. Jeon, B. A. Bernevig, and A. Yazdani, Observation of a Majorana zero mode in a topologically protected edge channel, Science **364**, 1255 (2019).
[68] Y. Peng and Y. Xu, Proximity-induced Majorana hinge modes in antiferromagnetic topological insulators, Phys. Rev. B **99**, 195431 (2019).
[69] Y.-J. Wu, J. Hou, X. Luo, Y. Li, and C. Zhang, In-plane Zeeman field Induced Majorana Corner and Hinge Modes in an s-wave Superconductor Heterostructure, Phys. Rev. Lett. **124**, 227001 (2020).
[70] C. M. Yue, Y. F. Xu, Z. D. Song, H. M. Weng, Y. M. Lu, C. Fang, and X. Dai, Symmetry-enforced chiral hinge states and surface quantum anomalous Hall effect in the magnetic axion insulator $Bi_{2-x}Sm_xSe_3$, Nat. Phys. **15**, 577 (2019).
[71] L. Fu and E. Berg, Odd-Parity Topological Superconductors: Theory and Application to $Cu_xBi_2Se_3$, Phys. Rev. Lett. **105**, 097001 (2010).
[72] M. Sato, Topological odd-parity superconductors, Phys. Rev. B **81**, 220504(R) (2010).

[73] S. Q. Shen, *Topological Insulators: Dirac Equation in Condensed Matter*, 2nd ed. (Springer, Singapore, 2017).

[74] S. Q. Shen, W. Y. Shan, and H. Z. Lu, Topological insulator and the Dirac equation, Spin **01**, 33 (2011).

[75] O. Vafek, Interacting fermions on the honeycomb bilayer: From weak to strong coupling, Phys. Rev. B **82**, 205106 (2010).

[76] L. Savary, J. Ruhman, J. W. F. Venderbos, L. Fu, and P. A. Lee, Superconductivity in three-dimensional spin-orbit coupled semimetals, Phys. Rev. B **96**, 214514 (2017).

[77] J. W. F. Venderbos, L. Savary, J. Ruhman, P. A. Lee, and L. Fu, Pairing States of Spin-3/2 Fermions: Symmetry-Enforced toPological Gap Functions, Phys. Rev. X **8**, 011029 (2018).

[78] See Supplemental Material at http://link.aps.org/supplemental/10.1103/PhysRevB.103.L180504 for details of the following: (Sec. SI) Symmetry of BdG Hamiltonian; (Sec. SII) Expansion of the interaction potential in Fermi-surface Harmonics; (Sec. SIII) Derivation of the Ginzburg-Landau free energy; (Sec. SIV) The multicomponents' basis functions in each representation; (Sec. SV) Spontaneous time reversal symmetry breaking for the mixed s and d wave pairing state; (Sec, SVI) Zero-temperature phase boundary for mixed $s + id$ wave pairing state; (Sec. SVII) Tight-binding model; (Sec. SVIII) The topological invariant for $s + id$ wave pairing state; (Sec. SIX) Possible relevance to the superconducting phases in transition-metal penta-telluride; and (Sec. SX) Comments on the repulsive interaction and disorder effect, which includes Refs. [75,76,79,80,86–90,93–101].

[79] T. Nomoto, K. Hattori, and H. Ikeda, Classification of multipole superconductivity in multiorbital systems and its implications, Phys. Rev. B **94**, 174513 (2016).

[80] M. Dresselhaus, *Applications of Group Theory to the Physics of Solids* (MIT Press, Cambridge, MA, 2002).

[81] G. Kotliar, Resonating valence bonds and d-wave superconductivity, Phys. Rev. B **37**, 3664 (1988).

[82] M. Liu, D. Y. Xing, and Z. D. Wang, Mixed $(s + id)$-wave order parameters in the Van Hove scenario, Phys. Rev. B **55**, 3181 (1997).

[83] P. J. Hirschfeld, Using gap symmetry and structure to reveal the pairing mechanism in Fe-based superconductors, C. R. Phys. **17**, 197 (2016).

[84] S.-Z. Lin, S. Maiti, and A. Chubukov, Distinguishing between $s + id$ and $s + is$ pairing symmetries in multiband superconductors through spontaneous magnetization pattern induced by a defect, Phys. Rev. B **94**, 064519 (2016).

[85] A. Benfenati, M. Barkman, T. Winyard, A. Wormald, M. Speight, and E. Babaev, Magnetic signatures of domain walls in $s + is$ and $s + id$ superconductors: Observability and what that can tell us about the superconducting order parameter, Phys. Rev. B **101**, 054507 (2020).

[86] C. A. Li, B. Fu, Z. A. Hu, J. Li, and S. Q. Shen, Topological Phase Transitions in Disordered Electric Quadrupole Insulators, Phys. Rev. Lett. **125**, 166801 (2020).

[87] B. Kang, K. Shiozaki, and G. Y. Cho, Many-body order parameters for multipoles in solids, Phys. Rev. B **100**, 245134 (2019).

[88] W. A. Wheeler, L. K. Wagner, and T. L. Hughes, Many-body electric multipole operators in extended systems, Phys. Rev. B **100**, 245135 (2019).

[89] H. Weng, X. Dai, and Z. Fang, Transition-Metal Pentatelluride $ZrTe_5$ and $HfTe_5$: A Paradigm for Large-Gap Quantum Spin Hall Insulators, Phys. Rev. X **4**, 011002 (2014).

[90] Y. Zhang, C. Wang, L. Yu, G. Liu, A. Liang, J. Huang, S. Nie, X. Sun, Y. Zhang, B. Shen, J. Liu, H. Weng, L. Zhao, G. Chen, X. Jia, C. Hu, Y. Ding, W. Zhao, Q. Gao, C. Li, S. He, L. Zhao, F. Zhang, S. Zhang, F. Yang, Z. Wang, Q. Peng, X. Dai, Z. Fang, Z. Xu, C. Chen, and X. J. Zhou, Electronic evidence of temperature-induced Lifshitz transition and topological nature in $ZrTe_5$, Nat. Commun. **8**, 15512 (2017).

[91] J. Mutch, W. C. Chen, P. Went, T. Qian, I. Z. Wilson, A. Andreev, C. C. Chen, and J. H. Chu, Evidence for a strain-tuned topological phase transition in $ZrTe_5$, Sci. Adv. **5**, eaav9771 (2019).

[92] B. Fu, H. W. Wang, and S. Q. Shen, Dirac Polarons and Resistivity Anomaly in $ZrTe_5$ and $HfTe_5$, Phys. Rev. Lett. **125**, 256601 (2020).

[93] Y. Zhou, J. Wu, W. Ning, N. Li, Y. Du, X. Chen, R. Zhang, Z. Chi, X. Wang, X. Zhu, P. Lu, C. Ji, X. Wan, Z. Yang, J. Sun, W. Yang, M. Tian, Y. Zhang, and H.-K. Mao, Pressure-induced superconductivity in a three- dimensional topological material ZrTe5, Proc. Nat. Acad. Sci. USA **113**, 2904 (2016).

[94] P. B. Allen, Fermi-surface harmonics: A general method for nonspherical problems. Application to Boltzmann and Kliashberg equations, Phys. Rev. B **13**, 1416 (1976).

[95] A. Altland and B. Simons, *Condensed Matter Field Theory* (Cambridge University Press, Cambridge, England, 2010).

[96] H. Fröhlich, Theory of the superconducting state. i. the ground state at the absolute zero of temperature, Phys. Rev. **79**, 845 (1950).

[97] J. Bardeen and D. Pines, Electron-phonon interaction in metals, Phys. Rev. **99**, 1140 (1955).

[98] P. Morel and P. W. Anderson, Calculation of the superconducting state parameters with retarded Electron-Phonon interaction, Phys. Rev. **125**, 1263 (1962).

[99] A. A. Abrikosov, L. P. Gorkov, and I. E. Dzyaloshinski, *Methods of Quantum Field Theory in Statistical Physics* (Dover, New York, 1975).

[100] P. W. Anderson, Theory of dirty superconductors, J. Phys. Chem. Solid **11**, 26 (1959).

[101] K. Maki, Gapless superconductivity, in *Superconductivity: Part II*, edited by R. D. Parks, (Marcel Dekker, New York, 1969).